Coherent Integration in Optical Interferometry

A. M. Jorgensen[a], H. R. Schmitt[b], G. T. van Belle[c], D. Mozurkewich[d], D. Hutter[e], J. T. Armstrong[f], E. K. Baines[f], S. Restaino[f], T. Hall[a]

[a]New Mexico Institute of Mining and Technology, Socorro, NM, USA
[b]Computational Physics, Inc., Springfield, VA, USA
[c]Lowell Observatory, Flagstaff, AZ, USA
[d]Seabrook Engineering, Seabrook, MD, USA
[e]Naval Observatory Flagstaff Station, Flagstaff, AZ, USA
[f]Naval Research Laboratory, Washington, DC, USA

ABSTRACT

Optical Interferometry has long been limited by low SNR making it nearly impossible to measure the small visibilities required to make resolved images. Although the SNR exists in the raw data, much SNR is lost in the conventional squared-visibility processing. In modern interferometers fringes are recorded simultaneously at many wavelengths and baselines. This makes phase-referencing possible, which is the key to coherent integration, which in turns can greatly improve the SNR of measurements, making small-amplitude resolving measurements possible. In this paper we will detail the theory of coherent integration. We will also explain why coherent integration should, in most cases, be carried out during post-processing in software rather than in real-time in hardware. We will then compare it to conventional processing approaches for some data from the Navy Optical Interferometer. We will demonstrate how coherent integration can improve the accuracy of observations.

1. INTRODUCTION

At visible and infrared wavelengths the atmosphere has a short coherence time of only a few milliseconds. Without strong active fringe tracking the fringes will move out of the range of the the beam combiner on a time-scale comparable to the coherence time. In many cases this time is too short to obtain sufficient signal-to-noise ratio for useful astronomical analysis. Instead many short observations, which freeze-frame the fringes, must be recorded and combined somehow. The traditional approach is to average the power spectrum of the fringes, which requires a bias subtraction. The bias that must be subtracted goes as $1/N$ where N is the number of photons recorded in one integration. For fainter targets the bias that must be subtracted is larger, and for targets with small visibilities the relative size of the bias to the signal is also large. Subtracting a large bias to obtain the astronomical quality degrades the SNR. In cases where NV^2 is small (typically smaller than unity), the degradation is large.

There is an alternative. If the individual exposures can be coherently averaged without a power-spectrum calculation the bias subtraction becomes much smaller because the noise is much smaller when squared visibilities are computed after long integrations.

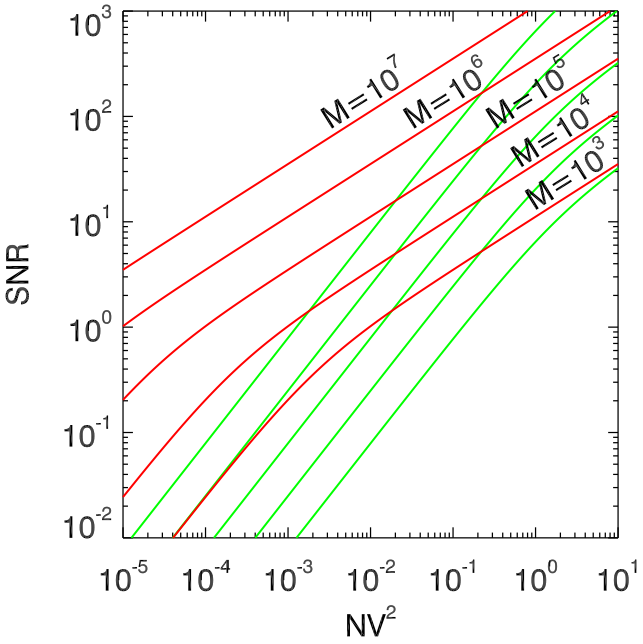

Figure 1. Signal-to-Noise ratio for coherent and incoherent observations of the same total duration. The green curves show the incoherent averaging SNR whereas the red curves show the coherent integration SNR.[1]

Optical and Infrared Interferometry III, edited by Françoise Delplancke, Jayadev K. Rajagopal, Fabien Malbet,
Proc. of SPIE Vol. 8445, 844519 · © 2012 SPIE · CCC code: 0277-786/12/$18 · doi: 10.1117/12.925898

Report Documentation Page

Form Approved
OMB No. 0704-0188

1. REPORT DATE	2. REPORT TYPE	3. DATES COVERED
JUL 2012		**00-00-2012 to 00-00-2012**

4. TITLE AND SUBTITLE	5a. CONTRACT NUMBER
Coherent Integration in Optical Interferometry	5b. GRANT NUMBER
	5c. PROGRAM ELEMENT NUMBER
6. AUTHOR(S)	5d. PROJECT NUMBER
	5e. TASK NUMBER
	5f. WORK UNIT NUMBER
7. PERFORMING ORGANIZATION NAME(S) AND ADDRESS(ES) **Naval Observatory Flagstaff Station,Flagstaff,AZ,86001**	8. PERFORMING ORGANIZATION REPORT NUMBER
9. SPONSORING/MONITORING AGENCY NAME(S) AND ADDRESS(ES)	10. SPONSOR/MONITOR'S ACRONYM(S)
	11. SPONSOR/MONITOR'S REPORT NUMBER(S)

12. DISTRIBUTION/AVAILABILITY STATEMENT
Approved for public release; distribution unlimited

13. SUPPLEMENTARY NOTES
Proc. of SPIE Vol. 8445

14. ABSTRACT

15. SUBJECT TERMS

16. SECURITY CLASSIFICATION OF:			17. LIMITATION OF ABSTRACT	18. NUMBER OF PAGES	19a. NAME OF RESPONSIBLE PERSON
a. REPORT **unclassified**	b. ABSTRACT **unclassified**	c. THIS PAGE **unclassified**	**Same as Report (SAR)**	**9**	

2. COHERENT INTEGRATION

Coherent integration means to integrate for a long time on the fringe while stabilizing the phase. The integration can be made long enough that sufficient SNR can be obtained from that single integration. This means that the complex visibility can be determined directly from single exposures. That in turn has a number of benefits including phase on every baseline and eliminating the need for squared visibility calculation with the related bias subtraction. In-fact, the greatest loss of signal-to-noise ratio in optical interferometry comes from bias subtraction.

3. SIGNAL-TO-NOISE RATIO

If we imagine observations with visibility V and N photons per short observations, and M short observations, then the SNR on the incoherent combination of those frames is[1]

$$\mathrm{SNR}_i = \frac{V^2}{\sigma_{V^2}} = \frac{\sqrt{M}}{4} \frac{NV^2}{\sqrt{1 + \frac{NV^2}{2}}} \tag{1}$$

If instead those MN photons are observed in a single frame (i.e. replace M with 1, and N with MN), then the expression for the SNR becomes

$$\mathrm{SNR}_c = \frac{1}{4} \frac{MNV^2}{\sqrt{1 + \frac{MNV^2}{2}}} \tag{2}$$

These two expressions are plotted in Figure 1 for as a function of NV^2 for different values of M. For the same values of M the red and green curves correspond to the same total integration time. However the green curves are the SNR of the incoherent averaging approach and the red curves are the SNR of the coherent integration approach.

We see that for small values of NV^2 the coherent integration approach produces far better SNR than the incoherent averaging approach, sometimes by orders of magnitude.

Another way to look at this information is by estimating the coherent integration time required to reach a particular SNR. That is essentially plotting M in equations 1 and 2. Figure 2 shows the required integration time for both incoherent averaging and coherent integration. As an example, to measure $NV^2 = 10^{-5}$ with a SNR = 10 would require 24 hours of integration time (perhaps of week of observing time) using coherent integration, but a thousand years of integration

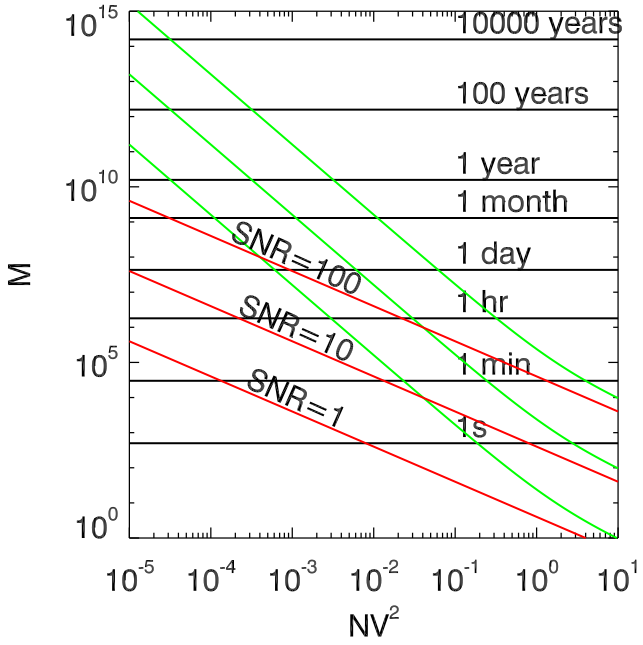

Figure 2. Integration time for several different levels of required SNR as a function of NV^2. The green curves are for incoherent averaging and the red curves are for coherent integration.

time using incoherent averaging. This makes the difference between possible (with coherent integration) and impossible (with incoherent averaging) observations.

4. PRACTICAL COHERENT INTEGRATION

In a practical optical interferometer coherent integration requires that the fringes can be tracked and the phase stabilized for the long integrations. There are several aspects of this to be considered.

4.1. Real-time or post-processing coherent integration

The first consideration is whether the coherent integration should take place in real time or during post processing. In real time coherent integration the fringes are stabilized by some external means such that fringes can be integrated on a detector such as a CCD. The phase reference must come from somewhere else, which we will discuss later in this section.

The primary difference between real-time and post-processing is in the timing of the phase information. In real-time coherent integration the phase information must be extrapolated from observations in the past whereas for post-processing coherent integration the phase information can be interpolated between the

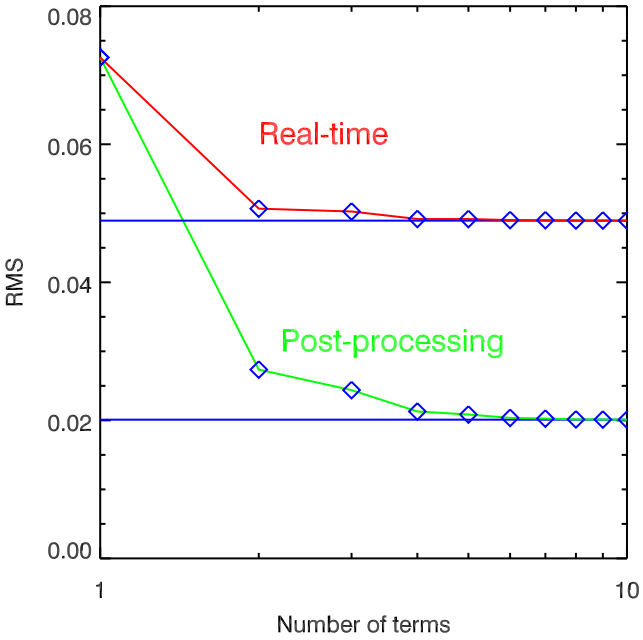

Figure 3. RMS prediction noise obtained from a Kalman filter of the phase for a real-time system (in red), and a post-processing system (in red). The horizontal axis is the number of terms in the Kalman filter.[2]

past and the future. Figure 3 shows the RMS phase error obtained from a Kalman filter. The red curve is for real-time system error and the green curve is for the post-processing system error. The horizontal axis is the number of terms in the Kalman filter. With only one term the two approaches are equal and use just the phase measured at the time before the observation. With two terms the real-time coherent integration does linear extrapolation whereas the post-processing system does linear interpolation for a greater reduction in phase error.

4.2. Baseline bootstrapping

Bootstrapping is a crucial component to coherent integration. It is the means by which the phase is transferred from where it is measured to phase-reference the photons being integrated. Even during post-processing bootstrapping must be used, because the photons which are being integrated may not be used to determine the phase reference. If they are used the effect will be to introduce a bias similar to the bias of the squared visibilities. The smaller the SNR of the frame, the larger the bias will be.

The most well-known approach to bootstrapping is baseline bootstrapping (Figure 4). In that case fringes are tracked on two or more baselines and used to stabilize the fringes on a baseline which is composed of them, using the closure relation,

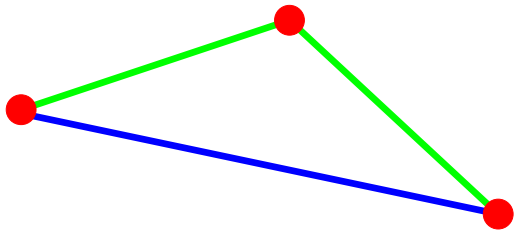

Figure 4. Illustration of a typical approach to baseline bootstrapping. In this case fringes are tracked on the two green baselines to stabilize the fringes on the blue baseline.

$$\phi_3 = \phi_2 + \phi_1 \tag{3}$$

where the ϕ_i is the phase on baseline i and the three baselines form a closure triangle. This approach is most often used when two shorter baselines with high SNR or NV^2 are combined to stabilize fringes on a baseline with small-amplitude fringes where coherent integration is needed in order to obtain required SNR in a shorter amount of time.

4.3. Wavelength bootstrapping

In addition to baseline bootstrapping it is also possible to use wavelength bootstrapping. In wavelength bootstrapping fringes at one or more wavelengths is used to track fringes at other wavelengths. We use the fact that the fringe phase varies in some systematic way with optical-path-difference (OPD) across wavelengths. For example, in the optical, the phase variation across wavelengths for given vacuum path, v, and air path, a, delays can be written as[1]

$$\theta = \frac{2\pi\left[v + (n-1)\,a\right]}{\lambda} \tag{4}$$

Because the index of refraction of air is so close to unity we usually subtract a constant from it (for example 1) and fold that into vacuum path delay to reduce the level of degeneracy between the two components. Vacuum path delay is a mis-match of the OPD in the vacuum delay lines of the interferometer, whereas air path delay can be caused by air pressure gradients along the physical baseline or residual air pressure in the delay lines or elsewhere in the system. In-fact we go a step further and subtract from $(n-1)$ its average value over the tracking band-pass (approximately 450 nm or 550 nm to 850 nm) to completely remove the degeneracy.

Equation 4 can be used to determine v and a from measured phases at a set or range of wavelengths, and then used to extrapolate or interpolate the phase at another set or range of wavelengths.

5. COHERENT INTEGRATION AT NPOI

At the NPOI[3] we use only post-processing coherent integration, and we used both wavelength and baseline bootstrapping. Since we have photon counting detectors the read-noise is zero and thus real-time coherent integration will actually yield worse SNR. We model the phase according to Equation 4. The cost function for determining v and a is to maximize the expression[4]

$$\left| \sum_{\lambda} V_{\lambda} e^{-i\theta} \right| \tag{5}$$

This optimization is carried out separately for the many thousands of frames in each of hundreds of scans in a night. To further increase the SNR of the determination of v and a we will sometimes combine multiple consecutive frames (for example 3 to 10) to interpolate the values of v and a for the central frame.[5] In that case we model the time-variation of v and a as low-order Legendre polynomials over the fixed interval of a few frames. This is computationally expensive and we have traditionally used supercomputers to do this computation. Recently we have implemented and tested algorithms for doing the optimization on General Purpose Graphics Precessing Units (GPGPUs).[6]

Since we should not integrate on the same photons that we track fringes on we will need to use wavelength bootstrapping and leave out the channels being integrated from the fringe-tracking. Figure 5 illustrates this. In panel (a) we have divided the wavelength channels into two sets, the odd channels and the even channels. We can track fringes on the even channels and use the determined values for a and v across all frames to coherently integrated the odd channels, and vice versa track fringes on the odd channels and use that to coherently integrate the even channels. In panel (b) we leave out one channel at a time and tracking fringes on the remaining 16 channels, then use that information to coherently integrate the channel that was left out. This is then repeated for every channel. Obviously the second approach uses more photons for fringe-tracking, but it comes at the cost of 15 times as much computation.

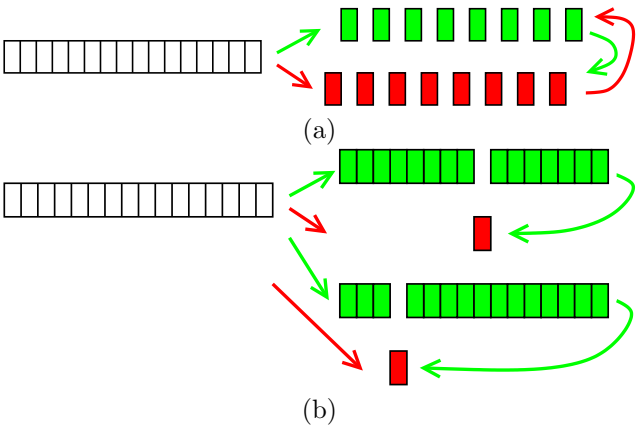

Figure 5. Illustration of two schemes for doing wavelength bootstrapping at the NPOI in order to avoid tracking fringes on the photons which are being coherently integrated. (a) a scheme in which the channels are divided into two sets, the odd and even channels. (b) a scheme in which the channels are divided into 16 (overlapping) sets, fringe-tracking on 15 channels to coherently integrate the remaining channel.

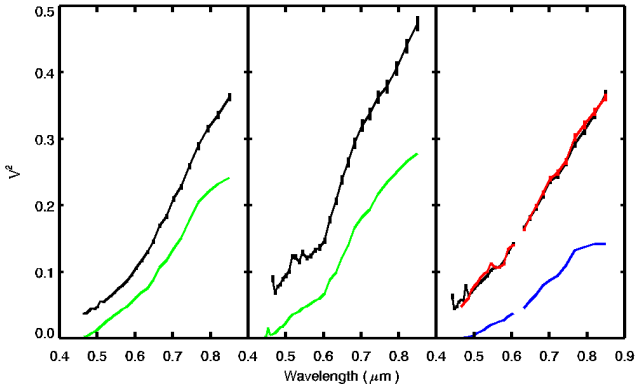

Figure 6. Illustration of amplitude calibration when using fringe-tracking of two high-SNR baselines to bootstrap a third baseline of (typically) low SNR.[1]

6. AMPLITUDE CALIBRATION

When we track fringes the determined fringe phase, as in equation 4 has finite SNR. That means that as we coherently integrate the fringes are smeared, which reduces the visibility amplitude. In order to make use of the coherently integrated visibilities we do, in most cases, need to correct for this amplitude reduction. More details of this are given in a companion paper.[7] If the phase noise is a Gaussian then the visibility reduction is[1]

$$\gamma = \int f(\theta) \cos\theta \, d\theta = e^{-\frac{\sigma^2}{2}} \tag{6}$$

where f represent a normalized Gaussian. The phase noise is not exactly Gaussian, but this description works

well under some circumstances. One scheme which has worked well is illustrated in Figure 6. A typical scenario where we might need to calibrate coherently integrated visibilities involves the case where we track fringes on two high-SNR baselines and baseline bootstrap the phase to a third baseline which is then coherently integrated,

$$\sigma_3^2 = \sigma_1^2 + \sigma_2^2 \tag{7}$$

We need to know the calibration factor of the third baseline. In this case the two tracking baselines will have sufficient SNR that the squared visibility, V^2, which is not smeared, can be computed. We can then measure the phase noise calibration factor as the ratio of the incoherently averaged to coherently integrated squared visibilities, compute the phase noise on the tracking baselines, σ_1, and σ_2q, and bootstrap to obtain the calibration factor on the bootstrapped baseline. In Figure 6 we illustrate this with three high-SNR baselines. Amplitude calibration is further discussed in other papers.[1,7]

7. DIAMETER MEASUREMENTS

With coherent integration the small amplitude visibilities in the vicinity of nulls in the visibility curve have better SNR than the squared visibility of the incoherent averaging approach. We can thus determine the location of the visibility null with greater precision when we use coherently integrated visibilities. The visibility null is a measure of the diameter of the star, we can in-fact call it the equivalent uniform-disk diameter of the star. We have been able to obtain very high precision with this approach, in a few cases better than 0.1% precision on diameters from only a few minutes of observations. And these diameters are wavelength dependent diameters where traditional analysis at the NPOI often folds in observations at all wavelengths of the spectrometer to improve SNR.

Recently we have also begun comparing these wavelength-dependent diameter measurements to stellar atmosphere models, in particular the Kurucz plane-parallel models. Figure 7 shows a model-data comparison for γ Sge. To do the comparison we started with the disk brightness distribution from the model and then computed the visibility and measured the location of the null. In that way we are simulating from the model exactly the same thing that we are measuring. While the overall slope is close in Figure 7, the spectral features from the model are not reproduces in the observations. Some of that difference is due to different

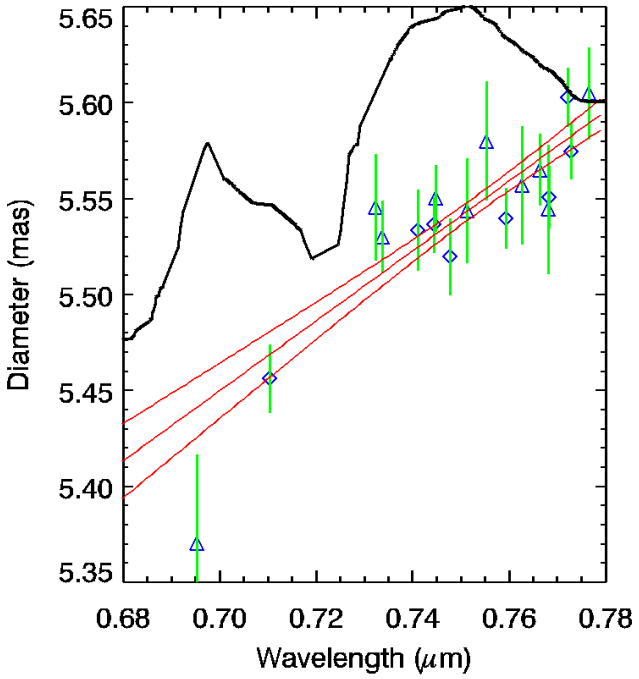

Figure 7. Diameter of γ Sge as a function of wavelength (blue symbols with green error bars), linear fit of the diameters as a function of wavelength (red curves, with uncertainty), and Kurucz model atmosphere diameter (black curve). The best diameters from the fit had a precision of approximately 0.1% between 0.75 and 0.76 μm.

wavelength bandwidths being used in the model and observations, but that cannot account for all of the difference. Additional results are available in a companion paper.[8]

8. IMAGING WITH COHERENT INTEGRATION

With coherent integration imaging becomes simpler. Coherently integrated visibilities are complex visibilities with the phase. This makes them appropriate for use in standard radio imaging packages such as AIPS or the follow-on CASA. Coherently integrated visibilities also obey Gaussian statistics instead of Poisson statistics, which is assumed by the radio imaging packages. On requirement, though, for imaging, is that that we have knowledge of the absolute phase, not simply relative phase. But the absolute phase can be obtained under the right circumstances.

Absolute phase can be determined on long resolving baselines which are bootstrapped from short non-resolving baselines. On the short non-resolving baselines we know that the phase is zero, and thus any phase obtained on the long baselines after bootstrapping will

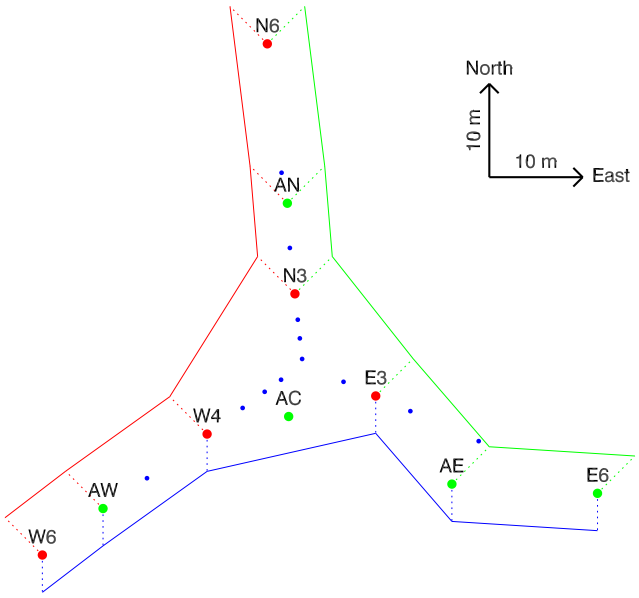

Figure 8. The NOI array layout to be used for this project. Green dots represent currently used telescope positions, red dots are locations to be commissioned for this project, and blue dots are other unpopulated piers. The three colored lines, offset from the telescope locations for clarity, represent the three six-station bootstrapping chains.

be the absolute phase. More details on interferometric imaging can be found in the paper by Schmitt et al.[9]

9. POSSIBLE FUTURE NPOI IMAGING ARRAY

To make use of the coherent integration and imaging capabilities that we have developed for NPOI over the years we have proposed a imaging array for the NPOI. To do the best imaging we should bootstrap long baselines from short baselines with as long a chain as possible. The NPOI can observe with 6 telescopes simultaneously so chains of 6 telescopes, or 5 baselines, is ideal. In Figure 8 we illustrates such an array of three 5-baseline 6-telescope chains. Its main design drivers were (1) to minimize new infrastructure and the number of piers that need to be commissioned, (2) to be a compact array which does not require the commissioning of the long delay lines, (3) be able to switch configuration between the three baselines of 6 telescopes without moving any telescopes, (4) have the shortest baselines be of approximately equal length. The array in Figure 8 satisfies most of those criteria. Criterium 4 is not fully satisfied as not all the shortest baselines are of equal length. This choice was made to minimize the cost and infrastructure required to bring the array up.

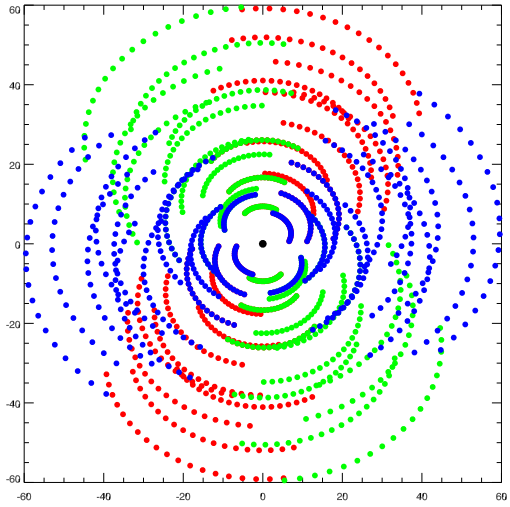

Figure 9. (u, v) coverage for the layout shown in Figure 8, with observations every 20 minutes during a 6-hour interval on each of the three bootstrapping chains. The color coding corresponds to the three chains in Figure 8. For convenience, the axes are indicated in meters; the actual spatial frequency for a given channel is B/λ.

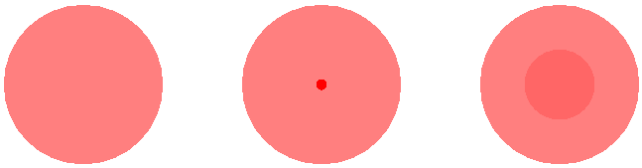

Figure 10. Three targets to be analyzed and differentiated. A limb-darkened disk (left), a limb-darkened disk with a small spot (center), and a limb-darkened disk with a large spot (right). The brightness of the spot is 3% of the brightness of the star, and the diameters of the stars is approximately 10 mas.

Figure 9 shows the UV coverage for the array at a single wavelength. This was produced by assuming 6 hours of observation on three different nights with observations every 20 minutes. This produces probably the most complete UV coverage of any optical interferometer to date, with large ratio of shortest to longest baselines. Note that this is a single-wavelength UV coverage. It can be compared with the much more spared multi-wavelength UV coverage that was used to produce a image of an eclipsing disk with MIRC.[10]

10. SNR CONSIDERATIONS FOR FUTURE NPOI IMAGING ARRAY

To illustrate the required SNR and need for coherent integration let's examine the observation of a few simple targets with the array depicted in Figure 8. Figure 10 shows three targets; a limb-darkened disk, a limb-darkened disk with a small spot, and a limb-

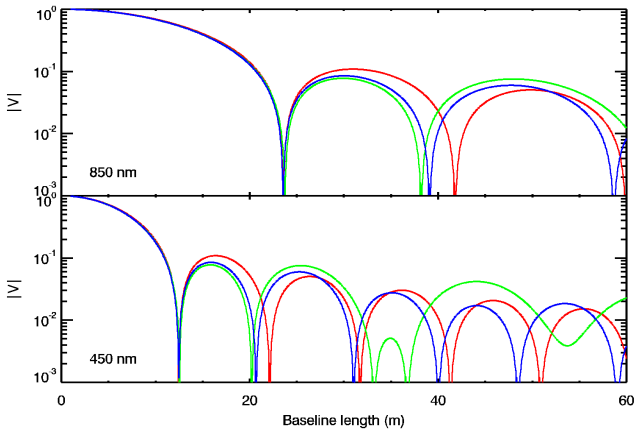

Figure 11. Visibilities for the three targets in Figure 10. The red curve is for the limb-darkened disk without a spot, the green curve for the limb-darkened disk with a small spot, and the blue curve is for the limb-darkened disk with the large spot. The top panel is for a wavelength of 850 nm, and the bottom is for a wavelength of 450 nm.

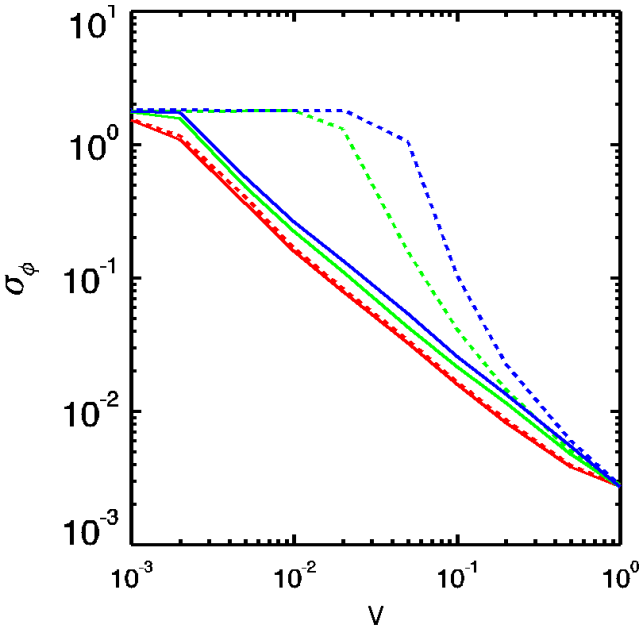

Figure 12. Phase noise for three different scenarios based on a simulation. Dashed curves are phase noise from incoherent averaging, whereas solid curves are phase noise from coherent integration. The red curves have two high-SNR baselines and one low-SNR baseline, the green curves have one high-SNR baseline and two low-SNR baselines, and the blue curves have three low-SNR baselines. The flattening of the curves at less than 2 radians is artificially due to phase wrapping. Correctly computed the phase noise continues to increase steeply for the dashed green and blue curves.[4]

darkened disk with a large spot. The spot adds 3% of the brightness of the main star, and the diameters of the targets are approximately 10 mas.

Figure 11 plots the visibilities for the three targets in Figure 10. The top panels is at 850 nm wavelength and the bottom at 450 nm wavelength. We see that in order to be able to differentiate the models substantially we need to look at the 4th lobe or beyond. The longest tracking (short) baseline is 18 m which results in a visibility amplitude of 0.2 in the first lobe at the longer wavelength. This is enough to track fringes.

Now assuming that we are looking at a faint target, the faintest 10 mas target that we can observe, what is the required integration time to be able to resolve the spot in the two cases, and distinguish the three cases? With 5 baseline bootstrapping we reach a maximum baseline length of 60 m which is the edge of the plot, so we will be able to measure the 4th lobe and beyond.

For fringe-tracking let's assume that we need SNR $= NV^2 = 10$ to track fringes. for $V = 0.2$ that means that we need at least 250 photons per 2 ms frame at the NPOI. This is an integrated number of photons across the 450-850 nm bandpass. With 32 channels that means 8 photons per channel. However almost all targets (and system transparency) produce far fewer photons in the blue than in the red. If we then assume 2 photons per coherence time in the far blue channels where we must resolve the spots. If we examine again Figure 11 we can see that we would need roughly to get SNR $= 10$ on $V = 0.01$. This is the end result. We start with $NV^2 = 2 \times 10^{-4}$ per frame in the blue channel. That comes from the two photons and the $V = 0.01$ value.

To find the required integration time we can examine again Figure 2. We find $NV^2 = 2 \times 10^{-4}$ on the horizontal axis and read off the total number of frames required, M, on the vertical axis for the required SNR for both coherent integration and incoherent averaging. With coherent integration the required SNR can be achieved after an hour or so of integration, which is still a very long integration time at the NPOI. With incoherent averaging on the other hand more than a year of integration time is required to reach the necessary SNR. For high-resolution imaging the difference between coherent integration and incoherent averaging can be the difference between a doable observation and a practically impossible observation.

11. PHASE IN IMAGING

Aside from the better SNR on the amplitude there is another reason to use coherently integrated visibilities. They produce better SNR on the phases as well. In incoherent averaging the phase can only be determined

with useful SNR from the triple products, V^3, of three baselines. The triple product has the same SNR problems as the squared visibility, V^2, only worse because of the higher order of the statistics. The SNR is much worse if the visibility amplitude is small on at least two of the baselines in the triangle, or more correctly, when the single frame SNR on at least two baselines is very small compared to unity.

Figure 12 compares the phase noise of coherently computed (solid) and incoherently computed (dashed) closure phases for three different scenarios. Red curves are for two high-SNR baselines and one low-SNR baseline, green curves are for one high-SNR baseline and two low-SNR baselines, and the blue curves are for three low-SNR baselines.

It is important to realize that when we work beyond the second null there will invariably be triangles which correspond to the green and blue low-SNR cases in Figure 12. This means longer integration times, in some cases such as illustrated in section 10 much longer integration times, when using incoherently averaged closure phases as opposed to either baseline phases or coherently obtained closure phases.

12. CONCLUSION

In this paper we have covered the main aspects related to coherent integration. We have described the theory of coherent integration and where it is applied, and the SNR gained from coherent integration. We have also given a description of the practical implementation of coherent integration at the NPOI. We outlined a case for a imaging array that makes use of the NPOI infrastructure with minimum additional investment, and showed that using such an array will allow sophisticated imaging, but requires coherent integration to obtain the required SNR.

ACKNOWLEDGMENTS

The NPOI is funded by the Office of Naval Research and the Oceanographer of the Navy. This work was supported by the National Science Foundation under grant 0909184. This work was also supported by New Mexico Institute of Mining and Technology and the Naval Research Laboratory.

REFERENCES

1. A. M. Jorgensen, D. Mozurkewich, H. Schmitt, T. Armstrong, C. Gilbreath, R. Hindsley, T. A. Pauls, and D. Peterson, "Coherent integrations, fringe modeling, and bootstrapping with the npoi.," Proc. SPIE 6268, Astronomical Telescopes and Instrumentation , 2006.
2. A. M. Jorgensen and D. Mozurkewich, "Coherent integration: to real time or not to real time? that is the question.," Proc. SPIE Astronomical Telescopes and Instrumentation , 2010.
3. J. T. Armstrong, D. Mozurkewich, L. J. Rickard, D. J. Hutter, J. A. Benson, P. F. Bowers, N. M. Elias II, C. A. Hummel, K. J. Johnston, D. F. Buscher, J. H. Clark III, L. Ha, L.-C. Ling, N. M. White, and R. S. Simon, "The Navy Prototype Optical Interferometer," Astrophys. J. **496**, pp. 550–571, 1998.
4. A. M. Jorgensen, H. R. Schmitt, J. T. Armstrong, D. Mozurkewich, E. K. Baines, R. B. Hindsley, D. Hutter, and S. R. Restaino, "Coherent integration results from the npoi," Proc. SPIE Astronomical Telescopes and Instrumentation , 2010.
5. A. M. Jorgensen, D. Mozurkewich, J. T. Armstrong, H. Schmitt, T. A. Pauls, and R. Hindsley, "Improved coherent integration through fringe model fitting," Astronomical Journal **134**, pp. 1544–1550, 2007.
6. M. Paiz and A. M. Jorgensen, "Coherent integration of optical interferometric data on a graphics processor," Proc. SPIE 8445, Astronomical Telescopes and Instrumentation , 2012.
7. T. Hall, A. M. Jorgensen, D. Mozurkewich, J. T. Armstrong, H. R. Schmitt, E. K. Baines, and D. Hutter, "Calibration of coherently integrated visibilities," Proc. SPIE 8445, Astronomical Telescopes and Instrumentation , 2012.
8. J. T. Armstrong, A. M. Jorgensen, H. R. Neilson, D. Mozurkewich, E. K. Baines, and H. R. Schmitt, "Precise stellar diameters from coherently averaged visibilities," Proc. SPIE 8445, Astronomical Telescopes and Instrumentation , 2012.
9. H. R. Schmitt, D. Mozurkewich, J. T. Armstrong, A. M. Jorgensen, E. K. Baines, S. R. Restaino, R. B. Hindsley, and G. van Belle, "Simulated imaging with an interferometer on a boom," Proc. SPIE 8445, Astronomical Telescopes and Instrumentation , 2012.
10. B. Kloppenborg, R. Stencel, J. D. Monnier, G. Schaefer, M. Zhao, F. Baron, H. McAlister, T. ten Brummelaar, X. Che, C. Farrington, E. Pedretti, P. J. Sallave-Goldfinger, J. Sturmann, L. Sturmann, N. Thureau, N. Turner, and S. M. Carroll, "Infrared images of the transiting disk in the ϵ aurigae system," Nature **464**, 2010.